Protein Science (1997), 6:2250–2260. Cambridge University Press. Printed in the USA.

^{1}H, ^{13}C, and ^{15}N backbone assignment and secondary structure of the receptor-binding domain of vascular endothelial growth factor

WAYNE J. FAIRBROTHER,[1] MARK A. CHAMPE,[1] HANS W. CHRISTINGER,[1]
BRUCE A. KEYT,[2] AND MELISSA A. STAROVASNIK[1]

[1]Department of Protein Engineering, Genentech Inc., South San Francisco, California 94080
[2]Department of Cardiovascular Research, Genentech Inc., South San Francisco, California 94080

(RECEIVED May 7, 1997; ACCEPTED May 20, 1997)

Abstract

Nearly complete sequence-specific ^{1}H, ^{13}C, and ^{15}N resonance assignments are reported for the backbone atoms of the receptor-binding domain of vascular endothelial growth factor (VEGF), a 23-kDa homodimeric protein that is a major regulator of both normal and pathological angiogenesis. The assignment strategy relied on the use of seven 3D triple-resonance experiments [HN(CO)CA, HNCA, HNCO, (HCA)CONH, HN(COCA)HA, HN(CA)HA, and CBCA-(CO)NH] and a 3D ^{15}N-TOCSY-HSQC experiment recorded on a 0.5 mM (12 mg/mL) sample at 500 MHz, pH 7.0, 45 °C. Under these conditions, ^{15}N relaxation data show that the protein has a rotational correlation time of 15.0 ns. Despite this unusually long correlation time, assignments were obtained for 94 of the 99 residues; 8 residues lack amide ^{1}H and ^{15}N assignments, presumably due to rapid exchange of the amide ^{1}H with solvent under the experimental conditions used. The secondary structure of the protein was deduced from the chemical shift indices of the $^{1}H^{\alpha}$, $^{13}C^{\alpha}$, $^{13}C^{\beta}$, and ^{13}CO nuclei, and from analysis of backbone NOEs observed in a 3D ^{15}N-NOESY-HSQC spectrum. Two helices and a significant amount of β-sheet structure were identified, in general agreement with the secondary structure found in a recently determined crystal structure of a similar VEGF construct [Muller YA et al., 1997, *Proc Natl Acad Sci USA 94*:7192–7197].

Keywords: chemical shift; protein secondary structure; resonance assignments; triple-resonance NMR spectroscopy; vascular endothelial growth factor

Vascular endothelial growth factor (VEGF) is a covalently linked homodimeric glycoprotein that functions as an endothelial cell-specific mitogen and is a potent angiogenic and vascular permeabilizing factor (Dvorak et al., 1995; Ferrara, 1995). Recent studies show that VEGF is a major regulator of developmental (Carmeliet et al., 1996; Ferrara et al., 1996) and reproductive (Phillips et al., 1990; Ravindranath et al., 1992; Shweiki et al., 1993) angiogenesis. VEGF is also an important mediator of blood vessel growth associated with cancer, rheumatoid arthritis, and proliferative retinopathy (Klagsbrun & D'Amore, 1991; Folkman & Shing, 1992; Aiello et al., 1994). Anti-VEGF antibodies are capable of suppressing the growth of tumors in nude mice (Kim et al., 1993) and also can inhibit angiogenesis in primate models of ocular neovascularization (Adamis et al., 1996). Antagonists of VEGF therefore have therapeutic potential to regulate pathological angiogenesis.

Reprint requests to: Wayne J. Fairbrother, Genentech, Inc., 1 DNA Way, South San Francisco, California 94080; e-mail: fairbro@gene.com.

Two receptors for VEGF have been characterized, Flt-1 (*fms*-like tyrosine kinase-1) (de Vries et al., 1992) and KDR/Flk-1 (kinase insert domain containing receptor/fetal liver kinase-1) (Terman et al., 1992; Millauer et al., 1993). Both receptors bind VEGF with high affinity ($K_d \sim 16$ and 760 pM for Flt-1 and KDR, respectively), although only KDR appears to have a mitogenic/angiogenic response (Waltenberger et al., 1994).

VEGF exists as four isoforms that result from alternative mRNA splicing, having 121, 165, 189, or 206 amino acids per monomer ($VEGF_{121}$, $VEGF_{165}$, $VEGF_{189}$, and $VEGF_{206}$, respectively) (Leung et al., 1989; Houck et al., 1991; Tischer et al., 1991). With the exception of $VEGF_{121}$, the different isoforms are highly basic and bind tightly to extracellular heparin or heparan sulfate-containing proteoglycans (Houck et al., 1992; Park et al., 1993). $VEGF_{165}$ is the isoform expressed most abundantly, and can be cleaved by plasmin to yield a 110-residue fragment, $VEGF^{1-110}$ (Keyt et al., 1996a). Proteolytic removal of the heparin-binding C-terminal domain has no effect on the ability of VEGF to bind KDR, but is associated with a significant loss in bioactivity, suggesting that the heparin-binding domain of $VEGF_{165}$ is required to sequester it to

the extracellular matrix (Keyt et al., 1996a). Limited sequence homology suggests that the receptor-binding domain ($VEGF^{1-110}$) is a member of the PDGF subfamily of the cystine-knot growth factor superfamily of proteins and, as such, is expected to dimerize in an antiparallel side-by-side fashion (Sun & Davies, 1995).

Two regions within the receptor-binding domain of VEGF have been identified by charged-to-alanine scanning mutagenesis as being important determinants for KDR and Flt-1 binding; positively charged residues close in sequence to Lys^{84} were found to be important for KDR binding, whereas negatively charged residues close in sequence to Glu^{64} were associated with Flt-1 binding (Keyt et al., 1996b). In addition, introduction of a glycosylation site at residue 84 was shown to block binding to KDR (Keyt et al., 1996b). A model of VEGF based upon the 3.0-Å resolution crystal structure of PDGF-BB suggests that Glu^{64} and Lys^{84} are distal in the monomer but proximal in the PDGF-like dimer (Keyt et al., 1996b). These results have been confirmed and extended recently by a more comprehensive alanine scan of these regions (Muller et al., 1997).

Due to the importance of VEGF in normal and pathological angiogenesis, we have undertaken structural analysis of the ~23-kDa receptor-binding domain of VEGF, comprising residues 11–109 of $VEGF_{165}$ ($VEGF^{11-109}$), in order to improve our understanding of its mechanism of action. As a necessary first step toward the determination of the solution structure of $VEGF^{11-109}$, we have completed the backbone ^1H, ^{15}N, and ^{13}C resonance assignments and determined the protein's secondary structure using both chemical shift and NOE information. While this work was in progress, a crystal structure of a similar receptor-binding domain construct ($VEGF^{8-109}$) became available (Muller et al., 1997), enabling us to compare the secondary structure observed in solution with that found by crystallography.

Results

Choice of construct

Preliminary homonuclear TOCSY spectra (τ_m = 30 ms) of the receptor-binding domain of VEGF obtained by plasmin cleavage of $VEGF_{165}$ ($VEGF^{1-110}$) (Keyt et al., 1996a), acquired at 40 °C, pH 6.5, in general showed only weak correlations between the amide and alpha protons. For a few residues, however, strong side chain-to-amide proton correlations were observed (data not shown). Assuming approximately random coil chemical shifts for the observed sharp side-chain signals indicated that they were most likely due to one each of Ala, Arg, Asp or Asn, Glu or Gln, and Met residues. The correspondence between these residue types and the residues at the N- and C-termini of the protein lead us to speculate that the eight N-terminal residues (Ala-Pro-Met-Ala-Glu-Gly-Gly-Gly) and two C-terminal residues (Asp-Arg) are highly flexible in solution. In an attempt to improve the quality of the NMR spectra and also to aid concurrent crystallization efforts, constructs comprising residues 8–109 ($VEGF^{8-109}$) and 11–109 ($VEGF^{11-109}$) of $VEGF_{165}$ were expressed and were determined by phage ELISA to have KDR-IgG binding affinities similar to that of $VEGF^{1-109}$ (Muller et al., 1997). The $VEGF^{8-109}$ construct resulted in crystals suitable for X-ray diffraction studies (Christinger et al., 1996), which have allowed the determination of its crystal stucture (Muller et al., 1997). $VEGF^{11-109}$ was selected for further NMR studies due to its slightly smaller size. Constructs having residues Glu^9 or Asn^{10} at their N-terminus were not considered good candidates for structural studies due to possible formation of pyroglutamic acid or deamidation of the asparagine residue, both of which could result in significant N-terminal heterogeneity.

NMR spectra

Sample conditions were selected on the basis of initial 1D and 2D ^{15}N-HSQC spectra of $VEGF^{11-109}$. At pH values below ~6.5, the protein precipitates. At protein concentrations greater than ~0.5 mM, increased linewidths, presumably due to concentration dependent aggregation, led to reduced sensitivity (e.g., HSQC spectra acquired using a 1.7-mM sample were less sensitive than those for the 0.5-mM sample). Analysis of chemical shifts in 1D spectra suggested that the protein is stable in the temperature range 30–50 °C, and for most residues linewidths decreased with increasing temperature. The solution conditions chosen for the experiments detailed below were therefore 0.5 mM protein (12 mg/mL), 25 mM sodium phosphate, 50 mM NaCl, pH 7.0, 45 °C, unless stated otherwise.

The ^{15}N-HSQC spectrum of $VEGF^{11-109}$ is shown in Figure 1. Although the cross peaks are broad, and several are clearly overlapping, 85 of an expected 91 backbone cross peaks (based upon a symmetric homodimer) could be identified; two of these were significantly weaker than the others, but had greater intensity in

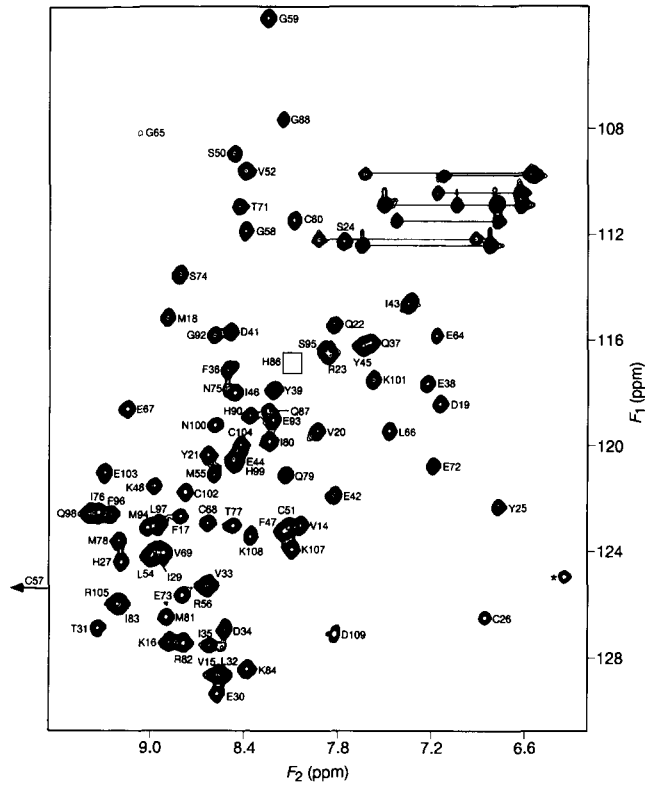

Fig. 1. ^{15}N-HSQC spectrum of ^{15}N-labeled $VEGF^{11-109}$ acquired at 45 °C, pH 7.0. The assignments obtained in this study are indicated. The cross peak for Cys^{57} is located outside the plotted region at F_1 = 125.7 ppm, F_2 = 12.09 ppm. The cross peak for His^{86} is broad and not observable at the level plotted in the figure; at a lower level, this peak is observable in the position indicated by the box. The cross peaks for Gly^{65} and His^{86} are significantly more intense at 35 °C. Side-chain amide resonances of Asn and Gln residues are connected by horizontal lines. The asterisk indicates a folded cross peak corresponding to an arginine $^1H^{\epsilon}$.

spectra acquired at a lower temperature, 35 °C, suggesting that they are broadened by rapid exchange with the solvent at the higher temperature. A third weak cross peak that did not show an increased intensity at the lower temperature was also identified. With the exception of the latter, all of the observed cross peaks were assigned using the 3D methods discussed below. Eight of the expected nine pairs of cross peaks corresponding to the side-chain amides of Asn and Gln residues were also identified.

Correlation time

Under the conditions used (0.5 mM protein, pH 7.0, 45 °C) the overall correlation time, τ_c, for the ~23-kDa homodimeric protein was estimated to be 15.0 ± 0.2 ns on the basis of ^{15}N R_2/R_1 ratios determined for 45 residues with well-resolved ^{15}N-HSQC cross peaks (average R_2/R_1 ratio = 15.9 ± 0.5; data not shown). For comparison, the value of τ_c calculated for VEGF$^{11-109}$ at 45 °C, assuming an approximately spherical molecule and a (typical) hydration of 0.3–0.4 g H_2O/g protein (Cantor & Schimmel, 1980), is 5.7 ± 0.3 ns. We attribute aggregation in solution as the major contributor to the larger than expected value of τ_c for VEGF$^{11-109}$, based upon the observed concentration dependence of the NMR linewidths. In addition, the shape of the molecule likely contributes to the elevated τ_c; the three principal components of the inertia tensor calculated from the crystal structure (Muller et al., 1997) have a ratio of 0.36:0.88:1.0. Indeed, the ^{15}N relaxation data are incompatible with isotropic rotational diffusion, but agree well with an axially symmetric rotational diffusion tensor with a diffusion anisotropy, $D_{\|}/D_{\perp}$, of 1.24 ± 0.04 using the method of Tjandra et al. (1995). The effective correlation time, $\tau_{c,eff}$, calculated from $1/(6D)$ is 14.8 ± 0.1 ns.

Backbone assignments

The size of the protein, coupled with the aggregation problems, the need to work at neutral pH, and the limitation of using a 500-MHz spectrometer, required that the triple-resonance experiments used for backbone assignment be as sensitive as possible. We therefore modified most of the triple-resonance experiments to include ^{15}N coherence selection using pulsed field gradients (Kay et al., 1992a; Muhandiram & Kay, 1994), which led to modest gains in sensitivity relative to nongradient-enhanced spectra, and provided excellent solvent suppression while avoiding saturation transfer losses from the amide protons. Nevertheless, a number of experiments used commonly to provide backbone correlations failed to give interpretable spectra for this sample; these include the CBCANH experiment (Grzesiek & Bax, 1992b), which can provide important intraresidue correlations between the amide ^1H and ^{15}N resonances and the $^{13}C^{\alpha}$ and $^{13}C^{\beta}$ resonances, and the HN(CA)CO experiment (Clubb et al., 1992a), which gives intraresidue correlations between the amide ^1H and ^{15}N resonances and the ^{13}CO resonance. Fortunately, the latter correlations could be obtained using the recently introduced (HCA)CONH experiment, which has significantly higher sensitivity than the HN(CA)CO experiment (Löhr & Rüterjans, 1995; Bazzo et al., 1996). Ultimately, seven triple-resonance spectra and a ^{15}N-TOCSY-HSQC spectrum were used to correlate the backbone nulcei and to obtain sequential resonance assignments (see Materials and methods; Table 2); example planes from these spectra, at a ^{15}N chemical shift of 122.9 ppm, are shown in Figure 2.

The spectral analysis was performed using the Assign module of FELIX 95.0. The strategy involved initial automated detection of spin-system patterns, using the sensitive HN(CO)CA spectrum for seed peak selection. New $^{13}C^{\alpha}$, ^{13}CO, and $^1H^{\alpha}$ chemical shifts were added to the individual spin-system patterns from the other 3D spectra if they had matching $^1H^N$ and ^{15}N chemical shifts. A complete spin-system pattern thus comprised chemical shift values for $^1H_i^N$, $^{15}N_i$, $^{13}C_i^{\alpha}$, $^1H_i^{\alpha}$, $^{13}CO_i$, $^{13}C_{i-1}^{\alpha}$, $^1H_{i-1}^{\alpha}$, $^{13}CO_{i-1}$, and $^{13}C_{i-1}^{\beta}$. In total, chemical shifts corresponding to 82 different patterns were identified, although not all patterns were complete due to missing peaks in some spectra. Only 64 of 82 expected $^{13}CO_i$ peaks were found in the (HCA)CONH spectrum (where the expectation is based upon the number of peaks observed in the more sensitive HN(CO)CA and HNCO spectra), 75 $^1H_{i-1}^{\alpha}$ peaks could be identified from the HN(CA)HA and HN(COCA)HA spectra, and 73 of an expected 77 (82 minus 5 Gly) $_{13}C_{i-1}^{\beta}$ peaks were observed in the CBCA(CO)NH spectrum. The total number of chemical shifts per pattern varied from 6 to 10, although the majority of patterns comprised 8 or 9 chemical shifts.

The patterns were linked sequentially by matching the $^{13}C_i^{\alpha}$, $^1H_i^{\alpha}$, and $^{13}CO_i$ chemical shifts of one pattern to the $^{13}C_{i-1}^{\alpha}$, $^1H_{i-1}^{\alpha}$, and $^{13}CO_{i-1}$ chemical shifts of another. In practice, the automated search was designed to match at least two of the three chemical shifts only, because not all of the patterns contained all of the potential shifts. Such a search yielded only 12 patterns with more than a single possible neighbor. In eight of these cases, a unique neighbor could be identified readily from the neighbor probabilities assigned by FELIX on the basis of the chemical shift matches. In all cases, manual inspection of all the available data, including the $^{13}C_{i-1}^{\beta}$ chemical shifts obtained from the CBCA(CO)NH spectrum, allowed the assignment of unique neighbors for all patterns, with the exception of 12, for which no neighbor could be identified. The latter correspond to the C-terminal residue, Asp^{109}, to residues N-terminal to proline residues (seven cases), or to those adjacent to residues for which no amide resonances were identified (four cases). The sequentially linked spin-system patterns were assigned to specific stretches of the protein sequence by amino acid typing on the basis of $^{13}C^{\alpha}$ and $^{13}C^{\beta}$ chemical shifts. In particular, glycine residues were identified readily from their $^{13}C^{\alpha}$ chemical shifts and by the observation of negative peaks in the (HCA)CONH spectrum, whereas serine and threonine residues were identified from their $^{13}C^{\beta}$ chemical shifts. In addition, the positions of proline residues were deduced from the $^{13}C_{i-1}^{\alpha}$ and $^{13}C_{i-1}^{\beta}$ chemical shifts of patterns that did not have identifiable N-terminal neighbors. Note that VEGF$^{11-109}$ contains no alanine residues, therefore easy identification of alanines on the basis of their distinctive upfield $^{13}C^{\beta}$ chemical shifts was of no benefit in this case. The correlations actually observed for each residue in the triple-resonance spectra are summarized in Figure 3.

At this stage of the assignment process, complete backbone assignments had been obtained for 86 residues; only two well-defined spin-system patterns and the peaks weakened due to solvent exchange (discussed above) remained unassigned. Residues i and $i-1$ from one of the unassigned patterns were determined to be an AM(PT)X spin-system (most likely a Glu or Gln) and an AMX spin-system, respectively, from analysis of a HCCH-TOCSY spectrum acquired from a D_2O sample; by elimination, this pattern was assigned to Glu^{64}. The amino acid type for residue i of the final unassigned pattern could not be determined from the HCCH-TOCSY spectrum due to overlap and sensitivity problems. However, the HCCH-TOCSY spectrum showed clearly the $i-1$ residue to be an AM(PT)X spin-system (Glu or Gln), allowing the assignment of this pattern to His^{90}. The HCCH-TOCSY spectrum was

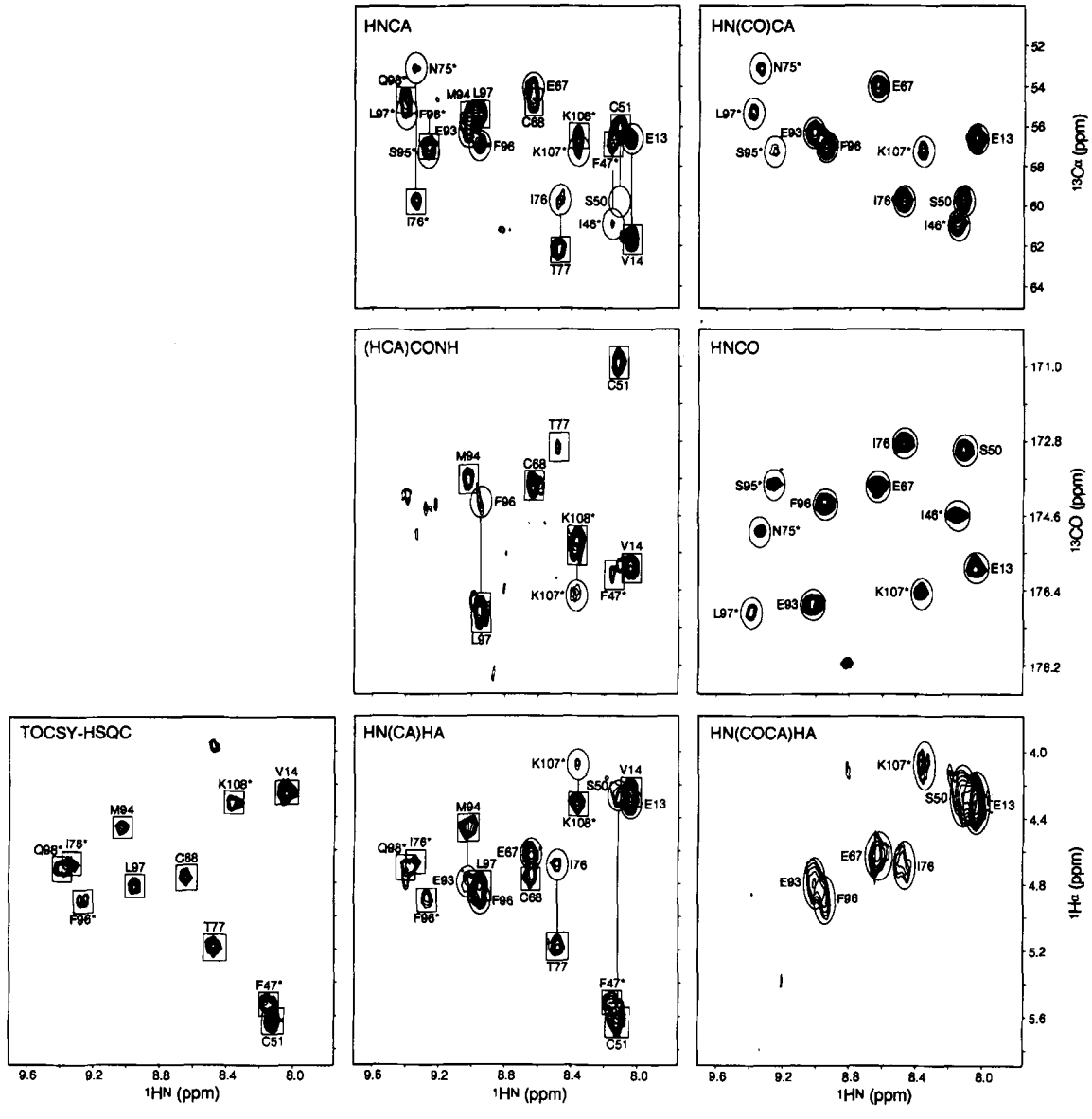

Fig. 2. Representative sections through the HNCA, HN(CO)CA, (HCA)CONH, HNCO, TOCSY-HSQC, HN(CA)HA, and HN(COCA)HA spectra of $^{15}N/^{13}C$-labeled $VEGF^{11-109}$, at a ^{15}N chemical shift of 122.9 ppm. Assignments obtained in this study are indicated. Intraresidue cross peaks are indicated by boxes and are labeled either above or below with the corresponding assignment. Interresidue ($i - 1$) cross peaks are indicated by ovals and are labeled to one side with the $i - 1$ assignment. Cross peaks having their maxima in an adjacent ^{15}N plane are indicated with asterisks (*).

also useful in confirming the amino acid types of other spin systems, but was not a necessity for assignment (except for Glu^{64} and His^{90} as stated). Two of the weak peaks observed in the ^{15}N-HSQC spectrum acquired at 45 °C were assigned to Gly^{65} and His^{86} on the basis of NOEs observed in a ^{15}N-NOESY-HSQC spectrum acquired at 35 °C, because these resonances are significantly sharper at the lower temperature.

The ^{1}H, ^{15}N, and ^{13}C assignments obtained for $VEGF^{11-109}$ are listed in Table 1. Complete backbone assignments were obtained for 90 of the 99 residues. Four of the remaining nine residues lack amide $^{1}H^{N}$ and ^{15}N assignments, but do have assignments for $^{13}C^{\alpha}$, $^{1}H^{\alpha}$, ^{13}CO, and $^{13}C^{\beta}$; five residues (His^{11}, His^{12}, Cys^{61}, Asn^{62}, and Pro^{85}) remain unassigned. Absence of these amide signals is most likely due to rapid exchange of the amide protons with the solvent at pH 7.0 and 45 °C (and 35 °C). Unfortunately, lowering the pH in order to reduce the amide proton exchange rates and thereby allow observation of the missing amide resonances is not a viable option for this sample due to poor solubility at lower pH values.

Four $^{1}H^{\alpha}$-$^{13}C^{\alpha}$ cross peaks in the 2D ^{13}C-HSQC spectrum are significantly sharper and more intense than the others, indicating that the corresponding residues are highly flexible in solution (data not shown). Two of these peaks correspond to Glu^{13} and the C-terminal residue, Asp^{109}; from analysis of the HCCH-TOCSY spectrum, the other two sharp peaks likely correspond to the N-terminal residues His^{11} and His^{12}, although specific assign-

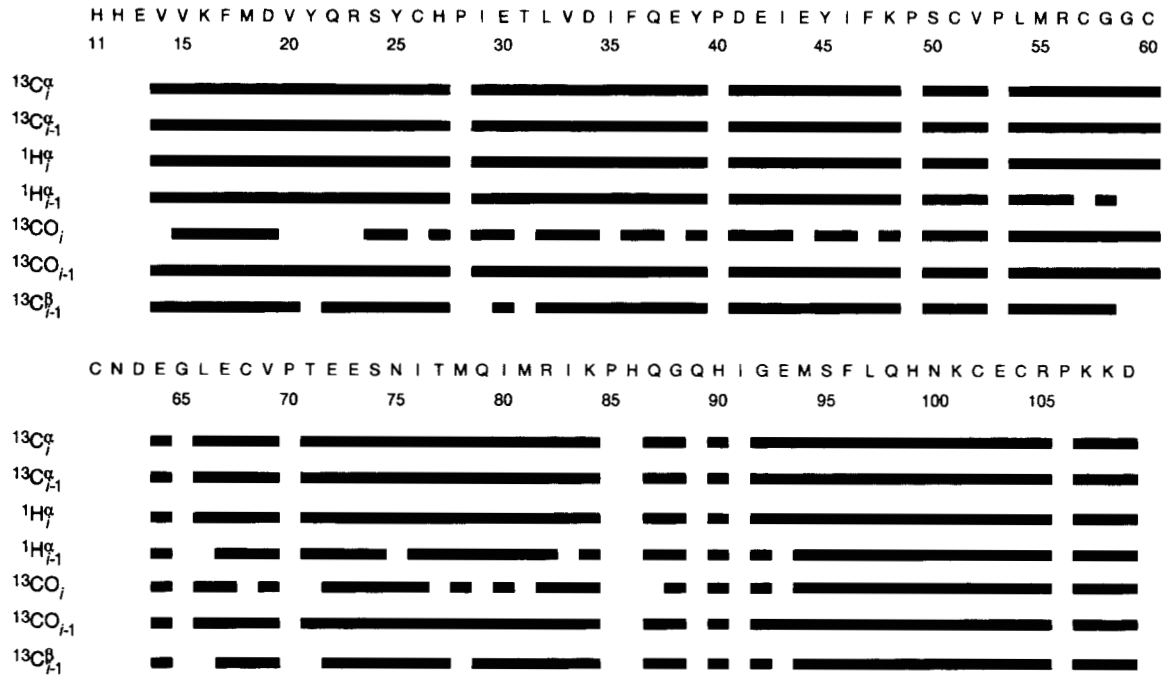

Fig. 3. Schematic representation of the correlations used for assignment of the backbone resonances. The presence of a cross peak for a residue is indicated by a bar. The correlations listed are found in the following experiments: $^{13}C_i^{\alpha}$, HNCA; $^{13}C_{i-1}^{\alpha}$, HN(CO)CA and/or HNCA; $^{1}H_i^{\alpha}$, TOCSY-HSQC and/or HN(CA)HA; $^{1}H_{i-1}^{\alpha}$, HN(COCA)HA and/or HN(CA)HA; $^{13}CO_i$, (HCA)CONH; $^{13}CO_{i-1}$, HNCO and/or (HCA)CONH; $^{13}C_{i-1}^{\beta}$, CBCA(CO)NH.

ments are not possible from the available data. Residues His[11], His[12], Glu[13], and Asp[109] were not included in the X-ray crystal structure model because no significant electron density was observed for these residues (Muller et al., 1997). Both the NMR and X-ray data are therefore consistent with these residues being flexible in solution.

Secondary structure

The $^{1}H^{\alpha}$, $^{13}C^{\alpha}$, ^{13}CO, and $^{13}C^{\beta}$ chemical shift assignments provide a convenient method to predict the secondary structure of VEGF[11–109] using the chemical shift index (CSI) method of Wishart and Sykes (1994a). The deviations of $^{1}H^{\alpha}$, $^{13}C^{\alpha}$, and ^{13}CO chemical shifts from random coil values (Wishart & Sykes, 1994b), and the consensus CSIs calculated using the public domain CSI program (Wishart & Sykes, 1994a), are plotted versus residue number in Figure 4. Also shown schematically in Figure 4 is the secondary structure obtained from the X-ray crystal structure of VEGF[8–109] (Muller et al., 1997) using the program PROCHECK (Laskowski et al., 1993). In general, the agreement between the secondary structure predicted using the CSI method and that found in the X-ray crystal structure is good. The CSIs clearly show the presence of two α-helices and a significant fraction of β-sheet structure, although there is some discordance between the beginning and end points of the secondary structure elements predicted using the consensus CSIs and the crystal structure, and indeed between the predictions based upon the individual CSIs. For instance, from the crystal structure, strand β1 comprises residues 27–34, whereas the consensus CSI prediction includes residues 31–33 only; the individual CSIs for $^{1}H^{\alpha}$, $^{13}C^{\alpha}$, and ^{13}CO predict β-structure for residues 31–33, 31–33, and 24–33, respectively, whereas the $^{13}C^{\beta}$ CSIs predict coil for this region. However, closer inspection of the crystal structure reveals that strand β1 is not a regular β-strand and that some of the ϕ angles vary substantially from that expected for an ideal β-strand (i.e., $-139°$). In particular, the ϕ angles of Pro[28], Glu[30], and Asp[34] are all between -75 and $-60°$. A number of other discrepancies between the CSI predictions and the secondary structure determined from the crystal structure using PROCHECK can also be explained by nonideal ϕ and ψ angles. Similar observations were reported recently for a comparison between the CSI predicted secondary structure and the crystal structure of β-hydroxydecanoyl thiol ester dehydrase (Copié et al., 1996).

The secondary structure of VEGF[11–109] was also characterized by analysis of sequential, medium- and long-range NOEs involving backbone $^{1}H^{\alpha}$ and amide protons (Wüthrich, 1986) observed in an 80-ms mixing-time ^{15}N-NOESY-HSQC spectrum acquired at 45 °C. Examples of such NOEs are present in Figure 5, which shows strips taken parallel to the $F_1(^{1}H)$ axis for different $F_2(^{15}N)$ planes corresponding to residues 18–27. The observation of sequential NOE connectivities also provided confirmation of the assignments obtained using triple-resonance methods. A summary of the sequential NOE data obtained from this spectrum is given in Figure 6. The two helices are clearly indicated by the pattern of sequential d_{NN} and $d_{\alpha N}(i, i + 3)$ NOEs between residues 17 and 25, and 35 and 39, and correspond closely to the helices observed in the crystal structure between residues 17 and 24, and 35 and 38, respectively. Interestingly, some of the sequential NOES observed for helix 1 are rather weak (20–21 and 21–22), suggesting that there may be some disorder in the middle of the helix, although no disorder is apparent from the crystal structure. Greater than average ^{15}N R_2 relaxation rates measured for Tyr[21] and Gln[22] indicate that these residues are likely involved in conformational exchange processes occurring on a μs to ms time scale (data not shown). The

Table 1. *Backbone ^{15}N, ^{1}H, and ^{13}C, and $^{13}C^{\beta}$ chemical shifts of VEGF$^{11-109}$ at 45 °C, pH 7.0*

Residue	^{15}N	$^{1}H^{N}$	$^{13}C^{\alpha}$	$^{1}H^{\alpha}$	$^{13}C^{\beta}$	^{13}CO	Residue	^{15}N	$^{1}H^{N}$	$^{13}C^{\alpha}$	$^{1}H^{\alpha}$	$^{13}C^{\beta}$	^{13}CO
Glu 13			56.6	4.30	31.3	175.9	Asn 62	—	—	—	—	—	—
Val 14	123.0	8.04	61.7	4.27	33.9	175.8	Asp 63	—	—	55.6	4.59	38.5	173.6
Val 15	128.7	8.57	63.2	4.09	32.3	175.9	Glu 64	115.8	7.17	54.4	4.71	—	176.4
Lys 16	127.4	8.88	56.9	4.12	33.3	178.2	Gly 65	108.1	9.07	45.6	3.80, 4.14		174.0
Phe 17	122.7	8.81	61.3	4.59	40.1	176.4	Leu 66	119.4	7.47	53.5	4.95	45.8	175.2
Met 18	115.2	8.89	57.9	3.95	31.6	178.5	Glu 67	118.6	9.15	53.9	4.62	33.4	173.8
Asp 19	118.4	7.15	57.4	4.49	41.3	178.0	Cys 68	122.9	8.64	54.7	4.76	36.3	173.9
Val 20	119.4	7.93	66.7	3.43	—[a]	178.0	Val 69	124.0	8.92	58.0	4.82	—	172.7
Tyr 21	120.3	8.63	62.2	3.65	39.0	178.0	Pro 70			62.5	5.01	—	178.5
Gln 22	115.4	7.83	59.0	3.90	29.3	178.6	Thr 71	110.9	8.44	61.2	4.35	69.1	175.2
Arg 23	116.5	7.86	58.6	3.98	32.0	177.2	Glu 72	120.8	7.19	57.2	4.54	34.4	175.1
Ser 24	112.2	7.77	59.0	4.28	65.3	172.6	Glu 73	125.7	8.80	55.2	5.43	34.3	175.0
Tyr 25	122.3	6.77	59.7	4.36	38.8	175.3	Ser 74	113.5	8.81	57.9	4.69	65.4	172.6
Cys 26	126.5	6.86	55.9	4.65	39.0	171.6	Asn 75	117.8	8.51	53.1	5.76	41.9	175.0
His 27	124.4	9.19	55.5	4.76	—	170.5	Ile 76	122.5	9.33	59.7	4.68	42.6	172.9
Pro 28			63.3	4.21	—	175.5	Thr 77	123.0	8.47	62.2	5.18	69.8	173.5
Ile 29	124.0	8.98	59.4	4.47	42.8	175.3	Met 78	123.6	9.20	54.6	5.09	37.7	174.6
Glu 30	129.4	8.57	59.3	4.15	—	175.3	Gln 79	121.1	8.14	55.9	4.79	30.1	173.2
Thr 31	126.9	9.34	61.8	4.25	71.7	171.8	Ile 80	119.8	8.24	57.7	4.67	41.8	176.5
Leu 32	128.7	8.55	53.4	4.82	40.1	176.2	Met 81	126.5	8.90	56.0	4.60	34.1	174.1
Val 33	125.2	8.63	61.3	4.07	35.1	175.5	Arg 82	127.4	8.79	55.4	4.67	32.5	175.4
Asp 34	126.9	8.52	55.0	4.63	42.6	177.7	Ile 83	126.0	9.20	61.4	4.36	40.7	175.2
Ile 35	127.5	8.62	67.1	3.41	37.9	178.1	Lys 84	128.4	8.38	53.0	4.96	—	174.6
Phe 36	117.1	8.51	59.9	4.50	38.5	177.3	Pro 85			—	—	—	—
Gln 37	116.1	7.59	58.3	4.10	29.2	177.4	His 86	(116.7)[b]	(8.11)[b]	58.3	4.25	29.3	175.2
Glu 38	117.7	7.23	57.1	4.10	31.7	176.2	Gln 87	118.7	8.25	56.6	4.61	31.5	175.8
Tyr 39	117.9	8.22	56.9	4.87	—	173.5	Gly 88	107.6	8.15	45.7	3.94, 4.22		172.1
Pro 40			64.9	4.59	32.5	177.9	Gln 89	—	—	54.3	5.24	32.6	174.6
Asp 41	115.7	8.49	54.9	4.76	41.2	177.8	His 90	118.9	8.37	56.0	4.74	—	173.6
Glu 42	121.9	7.82	56.6	4.83	29.1	176.6	Ile 91	—	—	61.2	4.30	37.8	175.7
Ile 43	114.6	7.35	62.6	4.25	39.4	176.7	Gly 92	115.8	8.59	44.2	3.60, 4.56		171.8
Glu 44	120.5	8.47	57.8	4.11	30.5	175.8	Glu 93	119.0	8.22	56.3	4.76	31.5	176.7
Tyr 45	116.2	7.64	57.7	4.70	41.3	175.2	Met 94	123.1	9.02	55.4	4.46	38.1	173.7
Ile 46	118.0	8.46	60.9	4.19	40.4	174.6	Ser 95	116.4	7.88	57.2	5.40	62.2	173.8
Phe 47	123.2	8.15	57.0	5.51	43.1	175.9	Phe 96	122.6	9.26	57.0	4.91	45.9	174.3
Lys 48	121.5	8.98	53.5	4.60	—	174.8	Leu 97	123.0	8.95	55.4	4.82	44.4	177.0
Pro 49			63.9	4.77	—	173.9	Gln 98	122.6	9.39	54.6	4.70	33.1	174.1
Ser 50	108.9	8.47	59.6	4.27	64.5	173.1	His 99	120.7	8.47	52.9	5.16	34.0	174.3
Cys 51	123.0	8.11	56.0	5.62	39.9	170.9	Asn 100	119.2	8.59	54.2	4.69	40.7	175.0
Val 52	109.6	8.39	57.1	4.74	—	172.8	Lys 101	117.5	7.58	56.5	4.39	37.6	175.3
Pro 53			61.0	4.91	30.8	175.3	Cys 102	121.8	8.78	54.5	5.46	48.5	173.2
Leu 54	124.2	9.00	52.8	4.68	47.3	176.5	Glu 103	121.0	9.29	55.2	4.57	35.5	174.2
Met 55	121.1	8.59	53.9	4.77	31.6	176.8	Cys 104	119.9	8.42	57.0	5.23	44.8	174.6
Arg 56	125.3	8.65	52.3	4.54	34.7	176.4	Arg 105	125.9	9.22	53.2	4.92	—	173.4
Cys 57	125.7	12.09	57.2	4.31	39.8	175.2	Pro 106			63.6	4.66	32.4	177.2
Gly 58	111.8	8.39	44.6	3.61, 4.28		170.5	Lys 107	123.9	8.10	57.3	4.08	34.0	176.5
Gly 59	103.8	8.25	44.9	3.41, 4.53		173.9	Lys 108	123.4	8.36	56.6	4.32	33.7	175.3
Cys 60	111.4	8.08	53.2	5.23	—	175.1	Asp 109	127.1	7.82	56.2	4.36	—	180.8
Cys 61	—	—	—	—	—	—							

[a]A dash (—) indicates nuclei for which no resonance was observed.
[b]These assignments are based upon cross peaks observed in NOESY-HSQC spectra acquired at 35 °C, and should be considered tentative.

d_{NN} NOEs between residues 22 and 23, and 23 and 24, are not observed due to overlap with the diagonal peaks (Fig. 5).

The β-sheet secondary structure is well defined by stretches of strong sequential $d_{\alpha N}(i, i + 1)$ NOE connectivities together with long-range $d_{NN}(i, j)$ and $d_{\alpha N}(i, j)$ NOEs, as indicated schematically in Figure 7. On the basis of the observed NOEs, the β-sheet secondary structure is identical to that found in the crystal structure. An interesting feature of β-strands 4 and 5 is the presence of two adjacent "β-bulges" at residues Thr^{71} and Asn^{100}, characterized by strong $d_{NN}(i, i + 1)$ NOEs between Thr^{71} and Glu^{72}, and between Asn^{100} and Lys^{101}, respectively, which lead to changes in the register of the β-strands. This structural feature is common to other members of the cystine-knot growth factor family, such as PDGF (Oefner et al., 1992) and TGF-β2 (Daopin et al., 1993;

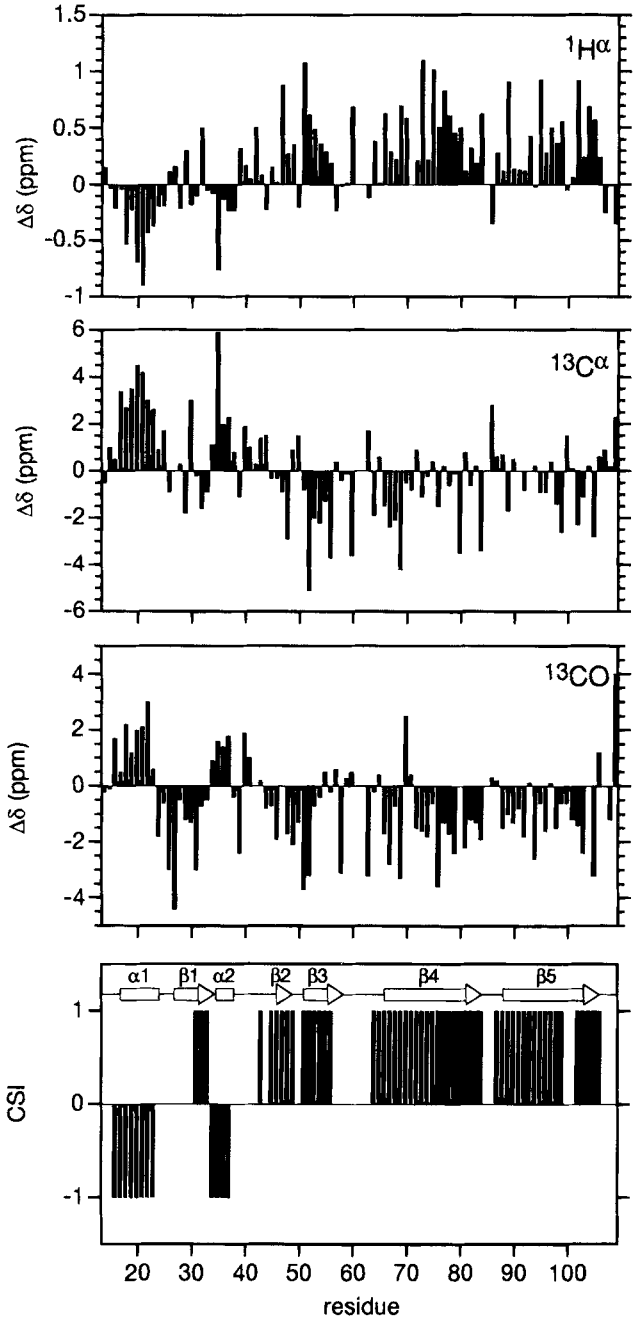

Fig. 4. Summary of the chemical shift deviations from random coil values for $^1H^\alpha$, $^{13}C^\alpha$, and ^{13}CO resonances, and the consensus CSI (bottom) for each residue in VEGF$^{11-109}$. The bottom panel also shows a schematic representation of the secondary structural elements as determined from the X-ray crystal structure of VEGF$^{8-109}$.

Schlunegger & Grütter, 1993). A break in the β-structure is indicated by the consensus CSI for the second of these two β-bulges (Asn^{100}-Lys^{101}), but not for the first (Fig. 4). In both cases, however, there is some disagreement between the consensus and the individual CSIs; the $^{13}C^\alpha$ CSI predicts coil for residues 71–75 and the ^{13}CO CSI predicts coil for residues 70 and 71, whereas both the $^1H^\alpha$ and $^{13}C^\beta$ CSIs predict β-structure for these residues; both $^1H^\alpha$ and $^{13}C^\alpha$ CSIs predict coil for residues 100 and 101, whereas the ^{13}CO and $^{13}C^\beta$ CSIs predict β-structure.

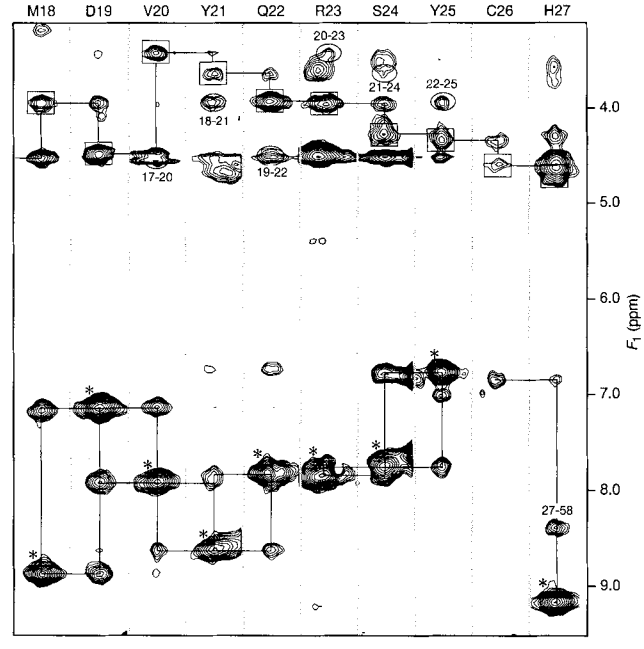

Fig. 5. Strip plot corresponding to selected regions of amide planes for residues 18–27 taken from an 80-ms mixing time ^{15}N-NOESY-HSQC spectrum of ^{15}N-labeled VEGF$^{11-109}$. The strips are arranged in sequential order, with the sequential assignment indicated at the top. Intraresidue $^1H^N$-$^1H^\alpha$ cross peaks, identified from a ^{15}N-TOCSY-HSQC spectrum, are boxed, and "diagonal" auto-correlation peaks are indicated by asterisks (*). Sequential d_{NN} and $d_{\alpha N}$ NOE correlations are indicated by lines to the diagonal and intraresidue $^1H^N$-$^1H^\alpha$ cross peaks, respectively; selected other medium- and long-range NOEs are labeled.

Backbone–backbone NOEs observed between residues Val^{15} and Met^{78}, and between Lys^{16} and Gln^{79} (Fig. 7) can be ascribed to intermonomer interactions via a hydrogen bond between Gln^{79} H^N and Val^{15} CO, as observed in the crystal structure. Observation of these and other NOEs confirms that the dimer orientation of VEGF$^{11-109}$ in solution is identical to that observed in the VEGF$^{8-109}$ crystal structure.

Discussion

Despite its highly unfavorable solution properties, almost complete backbone assignments have been obtained for VEGF$^{11-109}$ using ^{15}N- and ^{15}N/^{13}C-labeled samples and standard triple-resonance experiments acquired on a 500-MHz spectrometer. Although the nominal molecular mass of the VEGF$^{11-109}$ homodimer is ~23 kDa, the value of the overall correlation time, $\tau_c \approx 15$ ns, determined under the experimental conditions used for the spectral assignment (0.5 mM protein, pH 7.0, 45 °C) is evidence for significant protein aggregation. All of the triple-resonance experiments used provide correlations to the amide protons, thereby allowing assignment with a single ^{15}N/^{13}C-labeled sample in 90% H_2O/10% D_2O solution (note that, although a ^{15}N-TOCSY-HSQC spectrum acquired using a different ^{15}N-labeled sample was also used, it was not essential to the assignment process).

In most cases, the amide protons that remained unassigned due to absent cross peaks are found to be fully exposed to the solvent in the crystal structure, supporting our assertion that these protons are in rapid exchange with the solvent. An exception, however, is Cys^{61}, which is fully buried in the crystal structure. Absence of this

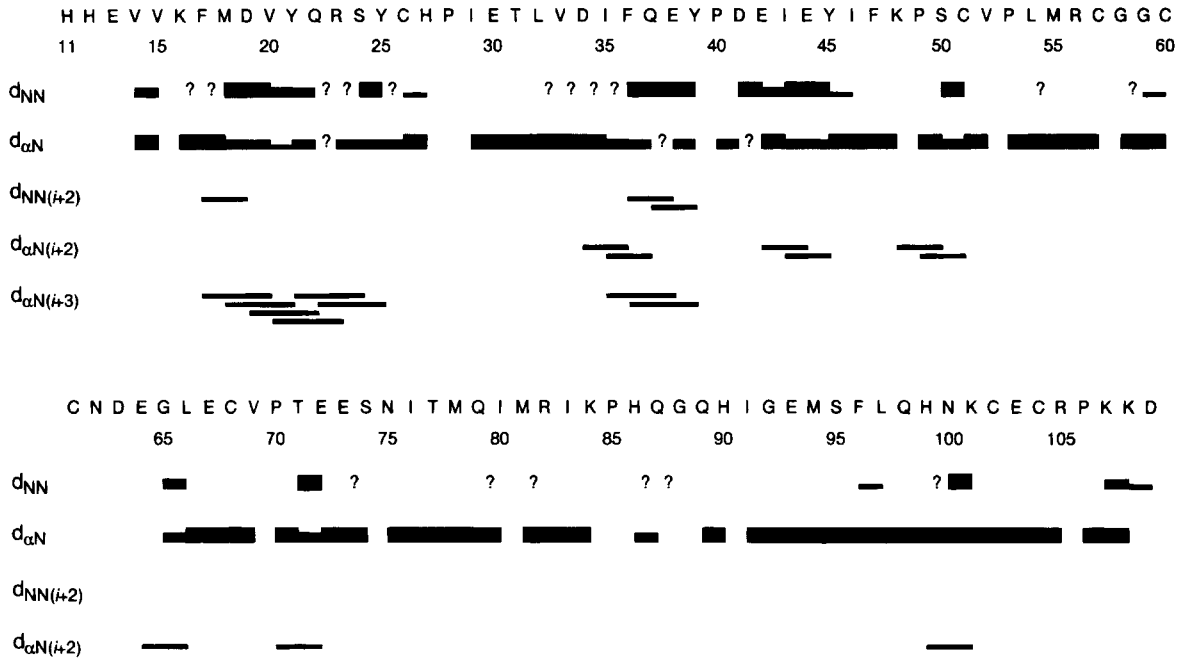

Fig. 6. Summary of the sequential NOE connectivities observed in the 80-ms mixing time ^{15}N-NOESY-HSQC spectrum of VEGF$^{11-109}$. The relative intensities of the sequential NOE correlations are indicated by the thickness of the bars between adjacent residues. Question marks indicate that a correlation could not be uniquely assigned due to overlap.

amide resonance suggests the possibility of conformational averaging of this cystine knot residue. Conformational averaging is also indicated for the amide of Cys^{26}, also a cystine knot residue, whose ^{15}N-HSQC cross peak broadens extensively upon reducing the temperature from 45 to 35 °C (data not shown).

Analysis of the backbone CSIs and NOEs allowed identification of the major secondary structure elements, generally in good agreement with the crystal structure. Discrepancies found between the CSI-based predictions and the NOE or crystallographically derived β-structure can be accounted for by irregularities present in the β-sheets of the crystal structure. The β-sheet secondary structure found for VEGF$^{11-109}$ resembles closely that observed in PDGF-BB (Oefner et al., 1992). However, the two helical regions identified in VEGF$^{11-109}$ near the N-terminus and immediately following β-strand 1, are not observed in PDGF-BB. In PDGF-BB, the N-terminal region is extended, whereas the conformation of the loop between β-strands 1 and 3 is not determined.

The secondary structure determined by NMR and X-ray crystallography reveals that the receptor-binding regions of VEGF, around Glu^{64} and Lys^{84} as identified by alanine scanning mutagenesis (Keyt et al., 1996b; Muller et al., 1997), are located at opposite ends of the major β-sheet (Fig. 7). The crystal structure further establishes that these two regions are proximal in the VEGF dimer (Muller et al., 1997), consistent with the previously pre-

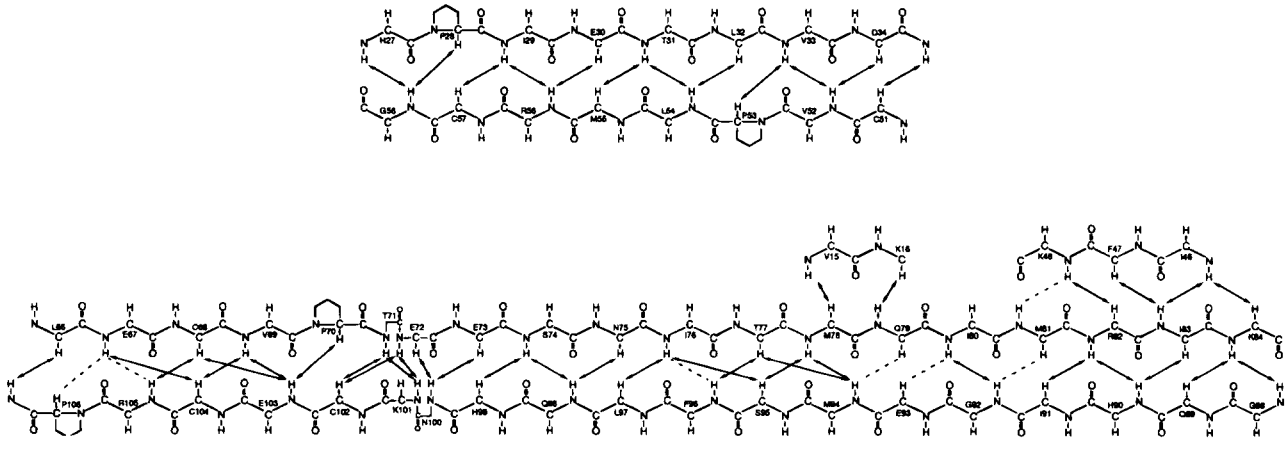

Fig. 7. Schematic representation of the antiparallel β-sheet secondary structure present in VEGF$^{11-109}$ as determined by analysis of NOE correlations. Observed interstrand NOE correlations are indicated by arrows. The dashed lines indicate ambiguous NOE correlations.

sented model of the VEGF receptor-binding domain (Keyt et al., 1996b). This information, together with the NMR assignments obtained from the present study, will allow for the rapid identification of potential peptide and/or small molecule antagonists of VEGF by monitoring ligand-induced chemical shift perturbations (Shuker et al., 1996); such investigations are currently in progress in our laboratory. In addition, understanding of the structure/function relationships for VEGF will benefit from analysis of the protein's internal dynamics. This is currently in progress using data from ^{15}N relaxation measurements.

Materials and methods

Expression and purification of VEGF$^{11-109}$

A cDNA clone of human VEGF was used in a PCR reaction with the primers: 5′-CGCGGATCCGCAGCTCATTATCATCACGAAG TGGTGAAGTTCATG (forward) and 5′-GTATCTCCCGGGCTAG TCTTTCTTTGGTCTGCATTC (reverse). The PCR product was digested with *Bam*H I and *Xma* I and ligated to the vector pQE30 (Qiagen) also digested with *Bam*H I and *Xma* I. The coding region of the resulting plasmid, p6XHis-VEGF$^{11-109}$, was sequenced for verification. This construct allows for the expression of a protein comprising VEGF amino acids 11–109 with the sequence MRG SHHHHHHGSAAHY added at the N-terminus. The amino acid sequence AAHY is a recognition sequence for Genenase I, a modified subtilisin that cleaves the protein after the tyrosine (Carter et al., 1989), leaving the native VEGF sequence, in this case beginning at His^{11}. A stop codon, TAG, was inserted after VEGF residue Asp^{109} to produce VEGF$^{11-109}$.

Escherichia coli strain SB558 (S. Bass, unpubl. results) containing plasmid pMS421 (Graña et al., 1988) was transformed with p6XHis-VEGF$^{11-109}$. Protein was expressed on minimal M9 medium, except that $^{15}NH_4Cl$ (99.8% ^{15}N atom, Isotec) was substituted for NH_4Cl at 1.5 g/L and ^{13}C-glucose (99.3% ^{13}C atom, Isotec) was substituted for glucose at 5 g/L for ^{15}N and ^{13}C labeling, respectively. A BioFlow III (New Brunswick) fermentor with 2 L of the appropriate M9 medium containing 50 μg/mL carbenecillin was inoculated with 250 mL of an overnight shake-flask culture of SB558 containing p6XHis-VEGF$^{11-109}$ in the same medium. Growth conditions were 37 °C, 500 RPM agitation, and 4 L air/min. Expression was induced by the addition of 2 mM IPTG when the culture reached an OD_{600} of 4.0. At this time, an additional 5 g/L glucose was added to the culture. Fermentation was continued for an additional 4–6 h postinduction to give a final OD_{600} of 10.0–12.0.

The His-tagged protein was purified on Ni-NTA resin according to the protocol for denaturing purification provided with the QIAExpress kit (Qiagen). Briefly, cells were dissolved in 6 M guanidine HCl, 0.1 M NaH_2PO_4, 10 mM Tris, 10 mM 2-mercaptoethanol, pH 8.0. Cell debris was removed by centrifugation and the supernatant was stirred with Ni-NTA resin for 1 h at room temperature. The resin was then loaded onto a column and washed consecutively with: 6 M guanidine HCl, 0.1 M NaH_2PO_4, 10 mM Tris, pH 8.0; 8 M urea, 0.1 M NaH_2PO_4, 10 mM Tris, pH 8.0; 8 M urea, 0.1 M NaH_2PO_4, 10 mM Tris, pH 6.3. The protein was eluted with 8 M urea, 0.1 M NaH_2PO_4, 10 mM Tris, 0.5 M imidazole, pH 5.9.

Protein concentration was adjusted to 1 mg/mL with elution buffer based upon an estimated extinction coefficient $A_{280} = 0.47$ $mL \cdot mg^{-1} \cdot cm^{-1}$. The pH was adjusted to 8.0 and DTT was added to a final concentration of 20 mM. Reduction was allowed to proceed for at least 3 h at room temperature in the dark. The protein solution was then dialyzed extensively in 20 mM Tris, pH 8.4, 25 mM cysteine at 4 °C using 6,000–8,000 MWCO dialysis tubing. Dialysis was continued until at least 50% of the material was converted to dimer as determined by visual inspection of Coomassie-stained SDS-PAGE gels.

The N-terminal His-tag was removed by Genenase cleavage for 6 h at room temperature in the presence of 1 M NaCl, 1 mM EDTA, 0.02% NaN_3 using a 1:20 ratio (w:w) of Genenase:protein. The protein was further purified, following dialysis into 10 mM NaCl, 20 mM Tris, pH 7.5, on a Q-Sepharose FF column, pre-equilibrated in the same buffer. Protein was eluted with a 0.01–1.0-M NaCl gradient in 20 mM Tris, pH 7.5, over 100 min at 2 mL/min. Load, flow through, and peaks were analyzed by non-reducing SDS-PAGE. Pooled fractions were then concentrated to 5 mL in a Centriprep 10 (Amicon) and loaded onto a Sephadex-100 gel filtration column and run at 4 °C with a flow rate of 0.35 mL/min in phosphate buffered saline. The maximum final yield of VEGF$^{11-109}$ obtained using the above procedure was ~45 mg/L of starting culture. The protein was >99% pure by SDS-PAGE. Electrospray mass spectrometry was used to verify protein and to determine the extent of isotope labeling.

NMR spectroscopy

All spectra were acquired at 45 °C (unless stated otherwise) on a Bruker AMX-500 spectrometer, equipped with a Bruker 5-mm inverse triple resonance probe with X-, Y-, and Z-gradient coils, except for a ^{15}N-NOESY-HSQC spectrum that was recorded using a Nalorac 8-mm inverse triple resonance probe with a Z-gradient coil. Proton chemical shifts were referenced to internal 3-(trimethylsilyl)propane-1,1,2,2,3,3-d_6-sulfonic acid, sodium salt (DSS-d_6; Isotec), and ^{13}C and ^{15}N chemical shifts were referenced indirectly to DSS and liquid ammonia, respectively (Wishart et al., 1995). Quadrature detection in the indirectly detected dimensions of all experiments was achieved using the States-TPPI method (Marion et al., 1989a). The acquisition parameters used for each experiment are summarized in Table 2. The ^{15}N-HSQC, TOCSY-HSQC, and NOESY-HSQC experiments were acquired using an ^{15}N-labeled sample; all other experiments were acquired using a double $^{15}N/^{13}C$-labeled sample. All triple resonance experiments, with the exception of the (HCA)CONH, were modified to include ^{15}N coherence selection via pulsed field gradients (Kay et al., 1992a; Muhandiram & Kay, 1994). Solvent suppression in the ^{15}N-HSQC and NOESY-HSQC experiments was achieved using the water "flip-back" method of Grzesiek and Bax (1993). In the TOCSY-HSQC and (HCA)CONH experiments, water suppression was achieved using a combination of spin-lock purge pulses (Messerle et al., 1989) and homospoil gradient pulses (Bax & Pochapsky, 1992). When required, WALTZ-16 (Shaka et al., 1983) was used for ^1H broadband decoupling and GARP-1 (Shaka et al., 1985) was used for ^{15}N decoupling during acquisition. In general, homonuclear ^{13}C decoupling ($^{13}C^{\alpha}$ or ^{13}CO) was achieved using selective 180° pulses.

Pulse sequences used to measure ^{15}N longitudinal and transverse relaxation rate constants (R_1 and R_2, respectively) were essentially as described previously (Stone et al., 1992; Skelton et al., 1993), except the sensitivity enhancement was achieved using the PEP-Z modification of Akke et al. (1994). Individual peak heights were measured for well-resolved cross peaks using macros written by Dr. Mikael Akke (Columbia University). The R_1 and R_2 values

Table 2. *Acquisition parameters for NMR experiments performed on VEGF$^{11-109}$*

Experiment	Acquired data matrix[a] (nucleus)			Spectral widths (Hz)			Number of transients
	t_1	t_2	t_3	F_1	F_2	F_3	
^{15}N-HSQC[b]	128 (^{15}N)	4,096 (^{1}H)		1,405	12,500		8–64
^{13}C-HSQC[c]	244 (^{13}C)	2,048 (^{1}H)		9,091	8,064		64
HN(CO)CA[d]	32 ($^{13}C^{\alpha}$)	24 (^{15}N)	2,048 (^{1}H)	3,125	1,165.5	8,064	64
HNCA[d]	32 ($^{13}C^{\alpha}$)	24 (^{15}N)	2,048 (^{1}H)	3,125	1,165.5	8,064	16
CBCA(CO)NH[e]	24 (^{13}C)	24 (^{15}N)	2,048 (^{1}H)	6,289	1,165.5	8,064	64
HNCO[d]	32 (^{13}CO)	24 (^{15}N)	2,048 (^{1}H)	1,509	1,165.5	8,064	32
(HCA)CONH[f]	16 (^{13}CO)	24 (^{15}N)	2,048 (^{1}H)	1,509	1,165.5	8,064	128
HN(COCA)HA[g]	9[k] ($^{1}H^{\alpha}$)	24 (^{15}N)	2,048 (^{1}H)	1,502	1,165.5	8,064	64
HN(CA)HA[h]	32 ($^{1}H^{\alpha}$)	24 (^{15}N)	2,048 (^{1}H)	1,502	1,165.5	8,064	64
^{15}N-TOCSY-HSQC[i] (τ_m = 39.5 ms)	128 (^{1}H)	24 (^{15}N)	2,048 (^{1}H)	5,000	1,165.5	8,064	16
^{15}N-NOESY-HSQC[i] (τ_m = 80 ms)	128 (^{1}H)	24 (^{15}N)	2,048 (^{1}H)	5,000	1,165.5	8,064	16
HCCH-TOCSY[j] (τ_m = 18.8 ms)	128 (^{1}H)	32 (^{13}C)	512 (^{1}H)	3,704	3,018	6,250	16

[a]Complex points.
[b]Bax et al. (1990b); Norwood et al. (1990).
[c]Vuister and Bax (1992).
[d]Grzesiek and Bax (1992c).
[e]Grzesiek and Bax (1992a).
[f]Löhr and Rüterjans (1995); Bazzo et al. (1996).
[g]Kay et al. (1992b).
[h]Clubb et al. (1992b); Kay et al. (1992b).
[i]Marion et al. (1989b).
[j]Bax et al. (1990a).
[k]Only nine complex points were acquired due to an untimely hardware failure.

and related uncertainties were determined by nonlinear least-squares fitting of the experimental data to monoexponential functions as described previously (Stone et al., 1992).

Spectra were processed and analyzed on a Silicon Graphics Indigo2 workstation, using the program FELIX 95.0 (Molecular Simulations). For the triple-resonance experiments [HN(CO)CA, HNCA, CBCA(CO)NH, HNCO, (HCA)CONH, HN(COCA)HA, and HN(CA)HA], linear prediction was used to extend the data by up to 50% in the indirectly detected dimensions. Zero-filling was employed in each dimension to yield final spectra of 64 (F_1) × 64 (F_2) × 2,048 (F_3) points, after discarding the upfield half of the spectrum in F_3 (i.e., the final F_3 spectral width is half the acquired spectral width listed in Table 1). For the ^{15}N-TOCSY-HSQC and NOESY-HSQC spectra, linear prediction and zero-filling were employed similarly to yield final spectra of 256 (F_1) × 64 (F_2) × 2,048 (F_3) points.

Acknowledgments

We thank Steve Bass for the *E. coli* strain and for advice on optimizing growth and expression conditions, Dorothea Reilly for advice on optimizing fermentation conditions, Brian Cunningham and Bing Li for performing binding assays, Arthur Palmer and Mikael Akke for providing Felix macros and programs used for analysis of relaxation data, Sandor Szalma for providing Felix macros for analysis of 3D NMR spectra, Yves Muller and Bart de Vos for sharing their coordinates of the VEGF$^{8-109}$ crystal structure prior to publication, and Nicholas Skelton for valuable discussions and critical reading of the manuscript.

References

Adamis AP, Shima DT, Tolentino MJ, Gragoudas ES, Ferrara N, Folkman J, D'Amore PA, Miller JW. 1996. Inhibition of vascular endothelial growth factor prevents retinal ischemia-associated iris neovascularization in a non-human primate. *Arch Ophthalmology 114*:66–71.

Aiello LP, Avery RL, Arrigg PG, Keyt BA, Jampel HD, Shah ST, Pasquale LR, Thieme H, Iwamoto MA, Park JE, Nguyen HV, Aiello LM, Ferrara N, King GL. 1994. Vascular endothelial growth factor in ocular fluid of patients with diabetic retinopathy and other retinal disorders. *N Engl J Med 331*:1480–1487.

Akke M, Carr PA, Palmer AG. 1994. Heteronuclear-correlation NMR spectroscopy with simultaneous isotope filtration, quadrature detection, and sensitivity enhancement using z rotations. *J Magn Reson B 104*:298–302.

Bax A, Clore GM, Gronenborn AM. 1990a. ^{1}H-^{1}H correlation via isotropic mixing of ^{13}C magnetization, a new three-dimensional approach for assigning ^{1}H and ^{13}C spectra of ^{13}C-enriched proteins. *J Magn Reson 88*:425–431.

Bax A, Ikura M, Kay LE, Torchia DA, Tschudin R. 1990b. Comparison of different modes of two-dimensional reverse-correlation NMR for the study of proteins. *J Magn Reson 86*:304–318.

Bax A, Pochapsky SS. 1992. Optimized recording of heteronuclear multidimensional NMR spectra using pulsed field gradients. *J Magn Reson 99*:638–643.

Bazzo R, Cicero DO, Barbato G. 1996. A new three-dimensional pulse sequence for correlating intraresidue NH, N, and CO chemical shifts in ^{13}C,^{15}N-labeled proteins. *J Magn Reson Ser B 110*:65–68.

Cantor CR, Schimmel PR. 1980. *Biophysical chemistry*. San Francisco: W.H. Freeman.

Carmeliet P, Ferreira V, Breier G, Pollefeyt S, Kieckens L, Gertsenstein M, Fahrig M, Vandenhoeck A, Harpal K, Eberhardt C, Declercq C, Pawling J, Moons L, Collen D, Risau W, Nagy A. 1996. Abnormal blood vessel development and lethality in embryos lacking a single VEGF allele. *Nature 380*:435–439.

Carter P, Nilsson B, Burnier JP, Burdick D, Wells JA. 1989. Engineering subtilisin BPN' for site-specific proteolysis. *Proteins Struct Funct Genet 6*:240–248.

Christinger HW, Muller YA, Berleau LT, Keyt BA, Cunningham BC, Ferrara N, de Vos AM. 1996. Crystallization of the receptor binding domain of vascular endothelial growth factor. *Proteins Struct Funct Genet 26*:353–357.

Clubb RT, Thanabal V, Wagner G. 1992a. A constant-time three-dimensional triple-resonance pulse scheme to correlate intraresidue $^{1}H^{N}$, ^{15}N and ^{13}C chemical shifts in ^{15}N-^{13}C-labeled proteins. *J Magn Reson 97*:213–217.

Clubb RT, Thanabal V, Wagner G. 1992b. A new 3D HN(CA)HA experiment for obtaining fingerprint H^{N}-H^{α} cross peaks in ^{15}N- and ^{13}C-labeled proteins. *J Biomol NMR 2*:203–210.

Copié V, Battles JA, Schwab JM, Torchia DA. 1996. Secondary structure of β-hydroxydecanoyl thiol ester dehydrase, a 39-kDa protein, derived from

H^{α}, C^{α}, C^{β} and CO signal assignments and the chemical shift index: Comparison with the crystal structure. *J Biomol NMR 7*:335–340.

Daopin S, Li M, Davies DR. 1993. Crystal structure of TGF-β2 refined at 1.8 Å resolution. *Proteins Struct Funct Genet 17*:176–192.

de Vries C, Escobedo JA, Ueno H, Houck K, Ferrara N, Williams LT. 1992. The *fms*-like tyrosine kinase, a receptor for vascular endothelial growth factor. *Science 255*:989–991.

Dvorak HF, Brown LF, Detmar M, Dvorak AM. 1995. Vascular permeability factor/vascular endothelial growth factor, microvascular hyperpermeability, and angiogenesis. *Am J Pathol 146*:1029–1039.

Ferrara N. 1995. The role of vascular endothelial growth factor in pathological angiogenesis. *Breast Cancer Res Treat 36*:127–137.

Ferrara N, Carver-Moore K, Chen H, Dowd M, Lu L, O'Shea KS, Powell-Braxton L, Hillan KJ, Moore MW. 1996. Heterozygous embryonic lethality induced by targeted inactivation of the VEGF gene. *Nature 380*:439–442.

Folkman J, Shing Y. 1992. Angiogenesis. *J Biol Chem 267*:10931–10934.

Graña D, Gardella T, Susskind MM. 1988. The effects of mutations in the *ant* promoter of phage P22 depend on context. *Genetics 120*:319–327.

Grzesiek S, Bax A. 1992a. Correlating backbone amide and side chain resonances in larger proteins by multiple relayed triple resonance NMR. *J Am Chem Soc 114*:6291–6293.

Grzesiek S, Bax A. 1992b. An efficient experiment for sequential backbone assignment of medium-sized isotopically enriched proteins. *J Magn Reson 99*:201–207.

Grzesiek S, Bax A. 1992c. Improved 3D triple-resonance NMR techniques applied to a 31 kDa protein. *J Magn Reson 96*:432–440.

Grzesiek S, Bax A. 1993. The importance of not saturating H_2O in protein NMR. Applications to sensitivity enhancement and NOE measurements. *J Am Chem Soc 115*:12593–12594.

Houck KA, Ferrara N, Winer J, Cachianes G, Li B, Leung DW. 1991. The vascular endothelial growth factor family: Identification of a fourth molecular species and characterization of alternative splicing of RNA. *Mol Endocrinol 5*:1806–1814.

Houck KA, Leung DW, Rowland AM, Winer J, Ferrara N. 1992. Dual regulation of vascular endothelial growth factor bioavailability by genetic and proteolytic mechanisms. *J Biol Chem 267*:26031–26037.

Kay LE, Keifer P, Saarinen T. 1992a. Pure adsorption gradient enhanced heteronuclear single quantum correlation spectroscopy with improved sensitivity. *J Am Chem Soc 114*:10663–10665.

Kay LE, Wittekind M, McCoy MA, Friedrichs MS, Mueller L. 1992b. 4D NMR triple-resonance experiments for assignment of protein backbone nuclei using shared constant-time evolution periods. *J Magn Reson 98*:443–450.

Keyt BA, Berleau LT, Nguyen HV, Chen H, Heinsohn H, Vandlen R, Ferrara N. 1996a. The carboxyl-terminal domain (111–165) of vascular endothelial growth factor is critical for its mitogenic potency. *J Biol Chem 271*:7788–7795.

Keyt BA, Nguyen HV, Berleau LT, Duarte CM, Park J, Chen H, Ferrara N. 1996b. Identification of vascular endothelial growth factor determinants for binding KDR and FLT-1 receptors. Generation of receptor-selective VEGF variants by site-directed mutagenesis. *J Biol Chem 271*:5638–5646.

Kim KJ, Li B, Winer J, Armanini M, Gillett N, Phillips HS, Ferrara N. 1993. Inhibition of vascular endothelial growth factor-induced angiogenesis suppresses tumor growth in vivo. *Nature 362*:841–844.

Klagsbrun M, D'Amore PA. 1991. Regulators of angiogenesis. *Annu Rev Physiol 53*:217–239.

Laskowski RA, MacArthur MW, Moss DS, Thornton JM. 1993. PROCHECK: A program to check the stereochemical quality of protein structures. *J Appl Crystallogr 26*:283–291.

Leung DW, Cachianes G, Kuang WJ, Goeddel DV, Ferrara N. 1989. Vascular endothelial growth factor is a secreted angiogenic mitogen. *Science 246*:1306–1309.

Löhr F, Rüterjans H. 1995. A new triple-resonance experiment for the sequential assignment of backbone resonances in proteins. *J Biomol NMR 6*:189–197.

Marion D, Ikura M, Tschudin R, Bax A. 1989a. Rapid recording of 2D NMR spectra without phase cycling. Application to the study of hydrogen exchange in proteins. *J Magn Reson 85*:393–399.

Marion D, Kay LE, Sparks SW, Torchia DA, Bax A. 1989b. Three-dimensional heteronuclear NMR of ^{15}N-labeled proteins. *J Am Chem Soc 111*:1515–1517.

Messerle BA, Wider G, Otting G, Weber C, Wüthrich K. 1989. Solvent suppression using a spin-lock in two- and three-dimensional NMR spectroscopy in H_2O solution. *J Magn Reson 85*:608–613.

Millauer B, Wizigmann-Voos S, Schnurch H, Martinez R, Moller NPH, Risau W, Ullrich A. 1993. High affinity VEGF binding and developmental expression suggest Flk-1 as a major regulator of vasculogenesis and angiogenesis. *Cell 72*:835–846.

Muhandiram DR, Kay LE. 1994. Gradient-enhanced triple-resonance three-dimensional NMR experiments with improved sensitivity. *J Magn Reson Ser B 103*:203–216.

Muller YA, Li B, Christinger HW, Wells JA, de Vos AM, Cunningham BC. 1997. Vascular endothelial growth factor: Crystal structure and functional mapping of the kinase domain receptor binding site. *Proc Natl Acad Sci USA 94*:7192–7197.

Norwood TJ, Boyd J, Heritage JE, Soffe N, Campbell ID. 1990. Comparison of techniques for ^{1}H-detected heteronuclear ^{1}H-^{15}N spectroscopy. *J Magn Reson 87*:488–501.

Oefner C, D'Arcy A, Winkler FK, Eggimann B, Hosang M. 1992. Crystal structure of human platelet-derived growth factor BB. *EMBO J 11*:3921–3926.

Park JE, Keller GA, Ferrara N. 1993. The vascular endothelial growth factor (VEGF) isoforms: Differential deposition into the subepithelial extracellular matrix and bioactivity of extracellular matrix-bound VEGF. *Mol Biol Cell 4*:1317–1326.

Phillips HS, Hains J, Leung DW, Ferrara N. 1990. Vascular endothelial growth factor is expressed in rat corpus luteum. *Endocrinology 127*:965–968.

Ravindranath N, Little-Ihrig L, Phillips HS, Ferrara N, Zeleznick AJ. 1992. Vascular endothelial growth factor mRNA expression in primate ovary. *Endocrinology 131*:254–260.

Schlunegger MP, Grütter MG. 1993. Refined crystal structure of human transforming growth factor β2 at 1.95 Å resolution. *J Mol Biol 231*:445–458.

Shaka AJ, Barker PB, Freeman R. 1985. Computer-optimized decoupling scheme for wideband applications and low-level operation. *J Magn Reson 64*:547–552.

Shaka AJ, Keeler J, Frenkiel T, Freeman R. 1983. An improved sequence for broadband decoupling: WALTZ-16. *J Magn Reson 52*:335–338.

Shuker SB, Hajduk PJ, Meadows RP, Fesik SW. 1996. Discovering high-affinity ligands for proteins: SAR by NMR. *Science 274*:1531–1534.

Shweiki D, Itin A, Neufeld G, Gitay-Goren H, Keshet E. 1993. Patterns of expression of vascular endothelial growth factor (VEGF) and VEGF receptors in mice suggest a role in hormonally regulated angiogenesis. *J Clin Invest 91*:2235–2243.

Skelton NJ, Palmer AG, Akke M, Kördel J, Rance M, Chazin WJ. 1993. Practical aspects of two-dimensional proton-detected ^{15}N spin relaxation measurements. *J Magn Reson B 102*:253–264.

Stone MJ, Fairbrother WJ, Palmer AG III, Reizer J, Saier MH Jr, Wright PE. 1992. Backbone dynamics of the *Bacillus subtilis* glucose permease IIA domain determined from ^{15}N NMR relaxation measurements. *Biochemistry 31*:4394–4406.

Sun PD, Davies DR. 1995. The cystine-knot growth-factor superfamily. *Annu Rev Biophys Biomol Struct 24*:269–291.

Terman BC, Dougher-Vermazen M, Carrion ME, Dimitrov D, Armellino DC, Gospodarowicz D, Böhlen P. 1992. Identification of the KDR tyrosine kinase as a receptor for vascular endothelial growth factor. *Biochem Biophys Res Commun 187*:1579–1586.

Tischer E, Mitchell R, Hartman T, Silva M, Gospodarowicz D, Fiddes JC, Abraham JA. 1991. The human gene for vascular endothelial growth factor. Multiple protein forms are encoded through alternative exon splicing. *J Biol Chem 266*:11947–11954.

Tjandra N, Feller SE, Pastor RW, Bax A. 1995. Rotational diffusion anisotropy of human ubiquitin from ^{15}N NMR relaxation. *J Am Chem Soc 117*:12562–12566.

Vuister GW, Bax A. 1992. Resolution enhancement and spectral editing of uniformly ^{13}C-enriched proteins by homonuclear broadband ^{13}C decoupling. *J Magn Reson 98*:428–435.

Waltenberger J, Claesson-Welsh L, Siegbahn A, Shibuya M, Heldin CH. 1994. Different signal transduction properties of KDR and Flt1, two receptors for vascular endothelial growth factor. *J Biol Chem 269*:26988–26995.

Wishart DS, Bigam CG, Yao J, Abildgaard F, Dyson HJ, Oldfield E, Markley JL, Sykes BD. 1995. ^{1}H, ^{13}C and ^{15}N chemical shift referencing in biomolecular NMR. *J Biomol NMR 6*:135–140.

Wishart DS, Sykes BD. 1994a. The ^{13}C chemical shift index: A simple method for the identification of protein secondary structure using ^{13}C chemical-shift data. *J Biomol NMR 4*:171–180.

Wishart DS, Sykes BD. 1994b. Chemical shifts as a tool for structure determination. *Methods Enzymol 239*:363–392.

Wüthrich K. 1986. *NMR of proteins and nucleic acids*. New York: John Wiley & Sons, Inc.